Highly radiating hydrogen flames: effect of toluene concentration and phase

M.J. Evans[a,*], D.B. Proud[a], P.R. Medwell[a], H. Pitsch[b], B.B. Dally[a]

[a] *School of Mechanical Engineering, The University of Adelaide, South Australia, 5005, Australia*

[b] *Institute for Combustion Technology, RWTH Aachen University, North Rhine-Westphalia, 52056, Germany*

Abstract

Adapting hydrogen as a carbon-free fuel for industrial applications requires new, innovative approaches, especially when radiant heat transfer is required. One possible option is to dope hydrogen with bio-oils, containing aromatics that help produce highly sooting flames. This study investigates the potential doping effects of toluene on a hydrogen-nitrogen (1:1 vol) flames. Flames with 1-5% toluene, based on the mole concentration of hydrogen, are measured using a combination of techniques including: still photographs and laser-based techniques. Toluene was mixed with hydrogen-nitrogen fuel mixture as either a vapour carried by nitrogen, or as a dilute spray. Spray flames are found to produce substantially more polycylic aromatic hydrocarbons, with significantly more soot near the nozzle exit plane, than the prevaporised flames. Increasing the dopant concentration from 1 to 3% of the hydrogen has a marked effect on soot loading in the flame, although the further increasing the dopant concentration to 5% has a far smaller effect

*Corresponding author. E-mail: m.evans@adelaide.edu.au, Tel.: +61 8 8313 5460, Fax: +61 8 8313 4367.

on the soot produced in the flame. Simulations of laminar flames using detailed chemical kinetics support the above findings and reveal details of the competition between soot precursor formation and hydrocarbon oxidation. Correlations of formation rates are non-linear with toluene concentration in cases where toluene represents less than 10% of the fuel, although expected linear relationships are noted beyond this regime up to 1:1 toluene/hydrogen blends. The study provides insight and explanation into effects of toluene as a dopant, comparison between flame doping in gaseous or liquid phases and suggests that flame doping and blending should be treated as different regimes for their global effect on flame sooting characteristics.
Keywords: Hydrogen, Toluene, Dual-fuel, Fuel dopants, Spray flames

---

1. Introduction

In the global shift towards a carbon-neutral economy, carbon-free fuels such as hydrogen and ammonia have been touted as sustainable, long-term alternatives to natural-gas and town-gas networks. Replacing natural- and town-gas with hydrogen in both domestic gas networks and at industrial scale poses technical challenges relating to the supply chain, the resulting flames, and the application of hydrogen to different industries. One such challenge is the low thermal radiation from pure hydrogen flames, especially in boiler and furnace applications. One approach to overcome this challenge is to dope the hydrogen fuel with a small amount of bio-oil to generate soot particulates within the flames to enhance radiative heat transfer and reduce both gas temperature and thermal NO_x formation.

Dual-fuel hydrogen and hydrocarbon combustion has been extensively studied as a fuel additive for enhancing combustion properties of less reactive or sooting fuels [1, 2]. Whilst numerous studies have demonstrated enhanced flame stabilisation and reduced soot loading through hydrogen addition with concentrations near 1:1 by volume [1, 3], there has been very little investigations of the effect of highly sooting hydrocarbon dopants ($\lesssim 5\%$ by mol.) on the sooting properties of near-pure hydrogen flames.

Toluene, and other aromatics, are prominent components of bio-oils [4]. Toulene has a high threshold sooting index (TSI) near 40 [5], which exceeds conventional, petroleum-derived diesel fuels at $\sim$30 [6]. Furthermore, toluene features in multiple combustion chemistry schemes for sooting fuels and is therefore suitable as a representative, highly-sooting dopant.

Toluene may be doped into hydrogen flames in its liquid or gaseous

phase—or a combination of both. The injection of fuel in its liquid phase as a dilute spray may reduce injection complexity without the need for pre-vapourisation, however, the liquid fuel droplets subsequently evaporate in the flame prior to and as part of combustion. Without the assistance of a hot pilot, the consequences of this difference in a simple gaseous jet flame are unknown and the effect on global flame characteristics are still to be determined.

The paper reports the characteristics of turbulent, attached, 1:1 hydrogen/nitrogen diffusion flames and the impact of toluene dopant, ranging between 1–5% of the mole concentration of H_2 (% mol_{H_2}), added as both a dilute spray or in vapour form. This series of flames allows for the independent investigations of the chemical effects of the toluene dopant on flame radiative characteristics and the physical effects of the liquid droplets in the dilute spray. Photographs of the flames are presented and analysed, as well as simultaneous, planar laser diagnostics. Analyses of trends and detailed measurements allow insight into the effects of highly-sooting dopants into otherwise carbon-free flames. This study further provides experimental data, including local soot concentration and spray penetration, to contribute towards validating future numerical simulations.

2. Methods

2.1. Burner Configuration

Turbulent flames issued from a 20 mm I.D. (D) pipe , surrounded by a 100 mm diameter coflow of room-temperature air at 0.33 m/s. The burner was operated in two different configurations, to allow toluene to be injected either as a liquid spray or as a vapour. For the spray flames, an ultrasonic

Table 1: Summary of flame conditions, including composition, jet exit temperature and stoichiometric mixture fraction (Z_{st}). All flames had 1:1 H_2:N_2 (by vol) with a pipe Reynolds number of 5,000. Toluene doping is based on the mole concentration of H_2 (only) in the jet stream.

Case	Toluene added (% mol_{H_2})	X_{H_2} (% total)	X_{N_2} (% total)	Initial toluene phase	Jet exit temperature (K)	Total heat input (kW)	Z_{st}
HT0	0.0	50	50	N/A	294	11.16	0.30
HT1-S	1.0	49.75	49.75	spray	294	11.17	0.28
HT3-S	3.0	49.25	49.25	spray	294	11.18	0.23
HT5-S	5.0	47.75	47.75	spray	294	11.20	0.20
HT1-V	1.0	49.75	49.75	vapour	300	11.17	0.28
HT3-V	3.0	49.25	49.25	vapour	300	11.18	0.23
HT5-V	5.0	48.75	48.75	vapour	300	11.20	0.20

nebuliser—which has been described previously [7]—was used to generate the toluene droplets with a nominal diameter of 40 μm. In the case of prevaporised toluene, a controlled evaporation and mixing (CEM) unit was installed upstream of the jet, with vaporised toluene carried by N_2 heated to 400 K. The difference in jet exit temperatures between the two cases was $\approx$6 K.

A 1:1 H_2/N_2 mixture (by mole) issued from the pipe with a fixed $Re = 5000$ for all flames. The addition of nitrogen facilitates higher values of Re in the relatively large-diameter pipe while also inhibiting soot formation, thus allowing the division between cases to be more clearly distinguished. Seven different attached flames were considered in this study; ranging from 0–5% toluene (C_6H_5-CH_3 or $A1CH_3$, where 'A' denotes an aromatic ring) addition (as a mole percentage of hydrogen in the fuel, denoted herein as % mol_{H_2}). It is worth noting that for these cases, the addition of toluene provides negligible heat input to the flame. Details of the flames are summarised in Table 1.

2.2. Experimental diagnostics

Simultaneous imaging of soot, liquid droplets, hydroxyl radicals (OH), and polycyclic aromatic hydrocarbons (PAH) was achieved using four separate laser diagnostic techniques at 10 Hz.

Prompt laser induced incandescence (LII) was used to measure the soot volume fraction (f_v), using the fundamental output of an Nd:YAG laser with a fluence of ~0.8 J/cm^2/pulse. This is in the plateau region [8] where measurements of f_v are expected to be insensitive to fluence for independent single-pulse measurements despite affecting soot morphology [9]. Incandescence from the soot was collected with an ICCD camera with a gate width of 100 ns through with an f/1.8 lens, and a 430 nm bandpass filter (FWHM 10 nm). The short camera gate of 100 ns ensured that transmitted chemiluminescence from CH* was below the detection limit and did not interfere with the LII signal. Similarly, emission from the C_2 Swan bands is at the periphery of the bandpass of the filter and was determined to have negligible impact on the LII measurements. Calibration was performed using laser extinction measurements at 1064 nm in premixed ethylene-air flames ($\Phi = 2.1$ and 2.3) stabilised on a McKenna burner [10].

Mie scattering of droplets using a 532 nm laser sheet with a pulse energy of 0.5 mJ was detected with a CCD camera through a 532 nm bandpass filter (FWHM 10 nm) and an f/5.6 lens with a 500 ns gate width. This technique allows for the observation of droplets but does not, in itself, facilitate droplet sizing.

Planar laser-induced fluorescence (PLIF) was used to detect the locations of both OH and PAH in the flame. OH-PLIF was performed with a

frequency-doubled dye laser, pumped by the 532 nm output of an Nd:YAG laser. The dye laser was tuned to the $Q_1(6)$ transition of the OH radical—with a measured energy of approximately 1 mJ/pulse. The resulting fluorescence was imaged using an ICCD camera through an f/3.5 UV lens and a 310 nm bandpass filter (10 nm FWHM, transmission $> 70\%$). Fluorescence of PAH was excited by the third harmonic (355 nm) of an Nd:YAG laser, with a measured energy of 120 mJ. This was imaged using another dedicated ICCD camera through a bandpass filter centred at 410 nm (FWHM of 10 nm), along with an f/1.2 lens. Both the OH and PAH cameras were operated with a gate width of 100 ns. The UV wavelengths used in this study may excite PAH [11] and toluene as a fuel (although this was not sufficiently strong to be measured in this study), with 355 nm lasers having previously been used in studies of CH_2O-LIF [12]. Some further interference from H_2 and H_2O Raman is possible, although an order of magnitude weaker than the PAH-LIF signal. As OH transition and was considered negligible for most measurements. This is discussed later in Section 5.

Beams were formed into sheets with a nominal height of 15 mm, overlapping similar to previous studies [13]. Mie scattering and PLIF pulses were each separated by less than 100 ns, with LII delayed by 400 ns to reduce interference. The in-plane resolution of the combined system was approximately 125 μm. A minimum of 250 image sets were captured for each flame case and measurement height. A 3×3 median filter was applied to the raw PLIF and LII images prior to image corrections to improve the signal-to-noise ratio. No filtering was used with Mie scattering images.

Photographs were taken with a DSLR camera using manual white-balance

and a series of multiple ISO, f-numbers and exposure times. Given the significantly different visibilities of the flames, it was not possible to maintain consistent settings for all cases and they are reported throughout.

2.3. Chemical Analyses

Numerical simulations and chemical analyses of axisymmetric, laminar opposed-flow flames were performed using Chemkin Pro v17.2 to complement the experimental observations. The chemical mechanism used was previously developed for modelling PAH formation, up to and including pyrene (A4), and includes 335 species and 1610 reversible reactions [14]. Naphthalene (A2) was chosen for analysis as a direct soot precursor because it: i) is the closest PAH in size to the fuel, simplifying the chemical pathways; ii) is often used as a direct soot precursor in numerical studies [15]; iii) fluoresces at the measurement wavelength under flame conditions [11]; and iv) is a key intermediate in A3 and A4 formation [15]. Comparative plots of modelled A3, A3 and A4 mole fractions are included as Supplementary Data.

3. Visual observations of toluene-doped hydrogen jet flames

Photographs of the flames are shown in Figs. 1 and 2. These are divided into long exposure images of all cases (Fig. 1) and short exposure images of the near-field of the doped flames (Fig. 2). Initial observations show that all flames that no burning toluene droplets escape the flame-front in the spray (HTx-S) cases. It is important to highlight that, although these photographs cannot provide quantitative planar or line data akin to LII, they can show radiation from soot volume fractions below the lower limit of the LII technique [16].

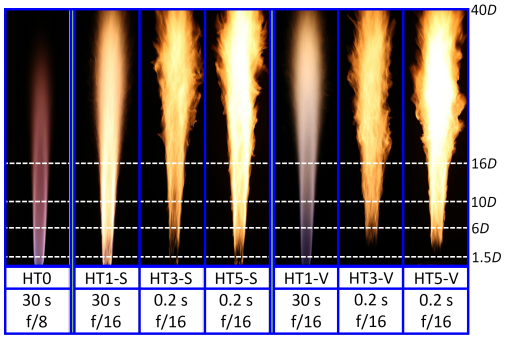

Fig. 1: Photographs of hydrogen and toluene-doped hydrogen flames with long exposures (exposure times and f-numbers provided below case-names). Photographs show 800 mm × 200 mm with the bottom of the images aligned with the jet exit plane. Several heights are labelled in multiples of D.

Flame photographs show the substantial changes in soot loading in all cases, even with minimal toluene doping of 1% by mol_{H_2}. The different exposure times required for the presented photographs is indicative of the impact of toluene on flame visibility. Although photographs of the toluene-doped flames are dominated by orange/yellow soot incandescence, non-sooting regions in these flames appeared blue due to the presence of CH*, C_2*, CO_2* and HCO*, with the red emissions in the pure H_2 flame (HT0) indicative of H_2O*.

Comparison of spray (HTx-S) and prevaporised (HTx-V) flames in Fig. 1 demonstrates the effects of toluene droplets on soot formation. It is notable that the spray flames all show earlier soot onset than the corresponding prevaporised cases, however, the HT3-S and HT5-S cases also exhibit peak intensity (and hence peak soot) further downstream than in their prevaporised counterparts. This suggests that some fraction of droplets burn shortly after leaving the jet exit plane. Other droplets persist downstream, gradually introducing toluene into the flame. Despite differences in the spatial

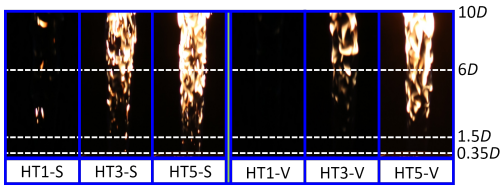

Fig. 2: Photographs of toluene-doped hydrogen flames with short (1 ms) exposures. Images were taken at f/16 with ISO-1600 and show 200 mm × 100 mm with the bottom of the images aligned with the jet exit plane. Several heights are labelled in multiples of D.

distribution of soot, the HT3 and HT5 flame-pairs (spray vs. prevaporised) appear to display similar radiative intensities, whereas the injection of 1% mol_{H_2} toluene as a dilute spray results in a higher soot-loading than as a prevaporised dopant.

Short exposure photographs in Fig. 2 highlight that individual droplets burn in isolation in the near-field of the flame, before the soot distribution becomes more homogeneous further downstream (Fig. 1). This is not dissimilar to the prevaporised flames, where soot kernels are identifiable upstream of larger soot sheets. These images demonstrate that toluene injected as a spray, rather than a vapour, results in earlier soot formation.

The soot around isolated droplets in the HTx-S flames (Fig. 2) is evidence of heterogeneous combustion driven by the evaporation of toluene. These high local concentrations are in contrast to the homogeneous distributions driven by the upstream mixing of the prevaporised fuel. In both circumstances, it is expected that the gaseous toluene forms dimers, which lead to the formation of larger PAH molecules and soot [13, 16]. It is not possible, however, to determine where droplet evaporation occurs relative to the reaction zone from photographs, leading to the necessity for simultaneous laser diagnostics.

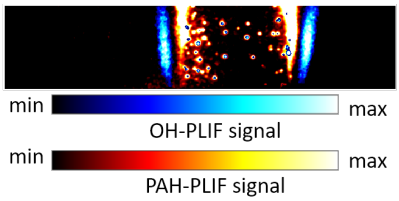

Fig. 3: Typical example of instantaneous fuel droplet distribution, soot precursors and OH-PLIF in dilute-spray-doped-flames (case HT5-S) centred at 0.3 x/D above the jet exit plane.

4. Extent of toluene droplets

A typical PLIF image of soot precursors, with fluorescence from liquid droplets, and OH is presented in Fig. 3. The figure shows that droplets consistently evaporate completely on the rich side of the reaction zone, without overlap with the OH layer. A negligible number of droplets escape through the preheat zone over the image set. The presence of soot precursors adjacent to the OH layer at the jet exit plane, however, demonstrates that some fuel vaporises before or at the jet exit plane. This further supports the flame and provides carbon-based radicals and intermediary species to the preheat zone. The fraction of liquid fuel which vaporises in the pipe varies with fuel, jet composition and momentum and has previously been estimated to be as little as 1–8% in methanol flames but 10–15% in ethanol flames in a similar burner [7]. The combination of these features indicates that the droplets are evaporating in high temperature regions of little-to-no-oxygen. This local deficiency of oxygen, or radicals such as OH, promotes the formation of soot which results in the features seen in Figs. 1 and 2. This effect does not occur in the flames doped with prevaporised toluene.

Complementing the analysis of the interactions between droplets and the

reaction zone in the near-field, Fig. 4 presents the droplet distribution along the dilute-spray-doped-flames. The curves in Fig. 4 show the normalised, radially-weighted number density of droplets at different downstream locations for the three dilute-spray-flame cases, which approximately follow an x^{-1} decay (where x is the height above the jet exit plane). The decay profiles in the absolute number of droplets (not shown) follow the same form. The associated planar images show the intermittency of droplets near the jet exit plane for the dilute spray-flames. These images show that droplets tend to cluster near the pipe walls before becoming more uniformly distributed downstream. This is consistent with the behaviour of low Stokes-number particles in pipe flow, resulting from Saffman lift and turbophoresis [17] which may assist in delivering smaller droplets to the near-field reaction zone, whilst carrying larger droplets further downstream. Figure 4 shows that liquid fuel is delivered as far downstream as 320 mm ($16D$) into the flame, even in the 1% dopant case, although the majority of droplets evaporate within the first 200 mm ($10D$). This equals the height of the photographs presented in Fig. 2 and highlights that not all droplets are a source of soot in the near-field, but contribute to more homogeneous soot downstream.

5. Effects of toluene-dopant on flame structure

Neither the addition of toluene as a vapour nor as a spray has a significant effect on the distribution of OH in the first 320 mm ($16D$) of the flames. This is shown by the consistency of the normalised mean OH-PLIF signal profiles at different downstream locations presented in Fig. 5. Non-zero signal on the centreline axis is indicative of LIF around the vapourising droplets in the near-field and PAH-LIF in highly sooting regions rather than OH-LIF.

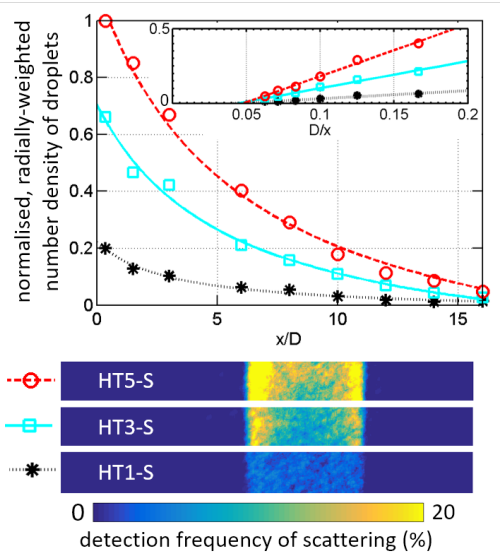

Fig. 4: Decay of radially-weighted droplet number density in dilute-spray-doped-flames, with linear, far-field x^{-1} trend inset. Below, planar images of the intermittency of Mie scattering signal centred at 0.3 x/D above the jet exit plane.

Despite the presence of interference near the centreline in downstream images of the highly sooting cases, the PAH and OH-PLIF regions are distinct in instantaneous images.

The mean profiles of OH-LIF signal in the spray (HTx-S) cases feature very similar magnitudes to the undoped flame, particularly near the jet exit plane. In contrast, the OH-LIF signal in the prevaporised (HTx-V) cases show a reduction in OH-LIF magnitude. This corresponds to a slight reduction in OH number density, supported by modelled trends presented as Supplementary Data, although the enhanced quenching effects of the gaseous toluene are expected to contribute to the reduction in the LIF signal. The spray cases, similarly, show the dopant addition has little impact on the magnitude of the OH-LIF signal and does not produce a second signal peak in

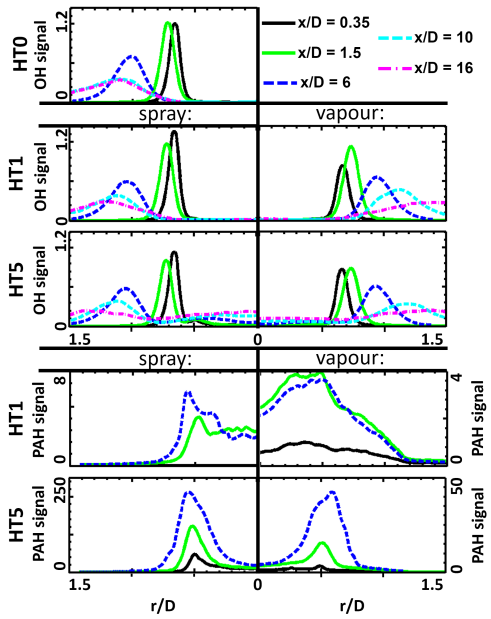

Fig. 5: Normalised OH-LIF and PAH-LIF profiles at different downstream locations in the doped and undoped flames. Flames are axisymmetric about $r/D = 0$ and plots of spray flame species distributions are flipped about the flame centreline to provide direct comparisons. All axes are linear. Note the different left-and-right-hand scales in the plots of normalised PAH profiles. OH-LIF is normalised by the peak signal in the HT0 flame centred at $x/D = 0.35$ and PAH-LIF is normalised by the peak signal in HT1-V centred at $x/D = 0.35$.

the profile, demonstrating the relatively small effect of toluene doping on the stabilisation and structure of the underlying H_2 flames.

In contrast to the OH radical, the PAH-LIF signal originates solely from the toluene dopant. The PAH-LIF signals presented Fig. 5 increase substantially with toluene concentration, but the signal is significantly stronger for the spray flames. This highlights the differences due to the dopant phase. Notably, the profiles demonstrate that the spatial extent of the preheat zone is largely unaffected by the toluene, which provides only a small amount of extra heat input.

6. Sooting propensity of toluene-doped flames

Toluene dopant in the H_2 flames may either form soot via PAH or be oxidised via CH_2O to produce CO_2. Although the desired effect of the toluene dopant is to enhance radiative heat transfer through the addition of soot in the flame, the high concentrations of OH from the H_2 combustion is likely to promote oxidation compared to conventional toluene diffusion flames. This was seen visually in Fig. 1, where the flames doped with 1% toluene exhibited significantly less visible soot incandescence compared to the HT3 and HT5 cases.

Comparison of f_v distributions at different heights above the jet exit plane (up to $16D$), in Fig. 6, confirm the enhanced formation of soot in the HT3 and HT5 flames compared to the HT1 cases. The prevaporised flames exhibit, in general, less measurable soot concentrations than the spray flames within this range. This is particularly highlighted by the magnitude and location of peak f_v, which is located closer to the jet centreline in the spray cases at $x/D = 6$ and 10. Multiple peaks at different r/D are present at $x/D = 16$, suggesting that the localised soot regions formed around individual droplets, as seen in photographs, persists downstream.

Figure 6 shows noticeable similarities in soot distribution between the HT3 and HT5 flames at $x/D = 10$ and 16, regardless of the dopant phase. This is due to the substantial evaporation of droplets by these heights (recall Fig. 4, showing that 95% of droplets vaporise upstream of $x/D = 16$). Local concentrations of f_v are critical in assessing the viability of toluene as a dopant to increase flame radiation. Correspondingly, Figure 6 suggests that $\sim$3% mol_{H_2} doping may be a lower threshold for substantially increasing

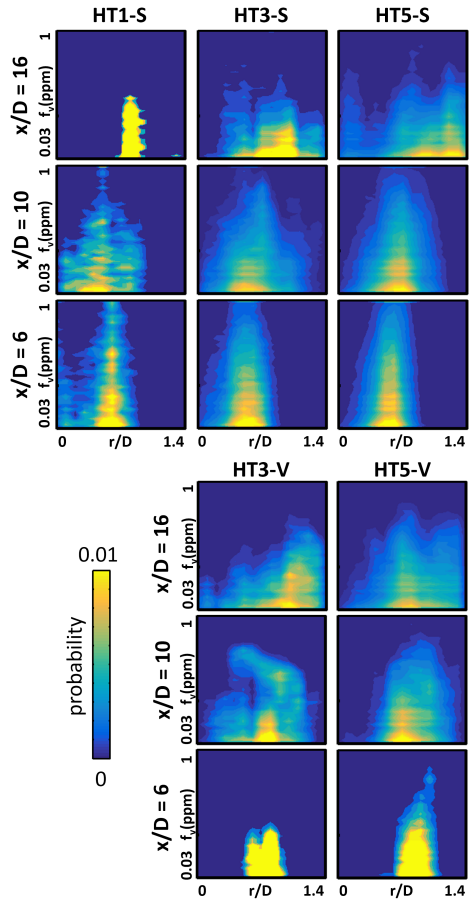

Fig. 6: Soot volume fraction PDFs (f_v in log-scale) at different heights in the doped flames taken over a 12 mm ($0.6D$) strip centred about the reported x/D. No soot was measured in the HT1-V case.

radiation in these H_2/N_2 flames, although the underlying mechanisms cannot be drawn from the experimental measurements alone.

Figure 7 shows the peak net absolute rates of production (ROPs) of CH_2O, A2 and the ratio of the two peak ROPs from the numerical analyses of opposed-flow diffusion flames, for both 0–10% (% mol_{H_2}) toluene dopant concentrations and from H_2-only to 1:1 H_2:toluene. As homogeneous

fuel mixtures, these represent prevaporised flames. The plots demonstrate the competition between toluene oxidation (via CH_2O) and soot formation (represented by A2 production [13]). An example reaction path diagram is provided as Supplementary Data. Although the tendency for soot formation appears to be linear with increasing toluene for large toluene:H_2 ratios, oxidation is strongly preferenced for very low toluene concentrations ($\lesssim$5% mol_{H_2}). Furthermore, the dominance of oxidation pathways in toluene-doped flames results in absence of net negative heat release rate regions. The preference for oxidation is driven by the high availability of OH and H from the reaction zone which promotes the oxidation of the CH_3 and A1 groups. As a result of this, the rate of A2 production increases by $\approx$650$\times$ between the HT1 and HT3 compositions, but by only $\approx$5$\times$ between HT3 and HT5. This latter difference is similar in magnitude to the increase between 5 and 10% mol_{H_2} toluene addition. The non-linear trend with dopant addition serves to explain the experimental differences in sooting propensity between the HT1-V case, and the HT3-V and HT5-V flames (Figs. 1, 2 and 6).

The behaviour of dopant-level concentrations of toluene is in contrast to large toluene-H_2 ratios ($\gtrsim$10% mol_{H_2}), hereafter referred to fuel blending rather than doping, where the relative rate of production of CH_2O to A2 indicates a preference for soot formation over oxidation. Although high relative concentrations of toluene do not occur in the homogeneous, prevaporised flames, high local concentrations of toluene occur around the evaporating droplets in the spray cases. The curve-fits in Fig. 7 are grouped into those for small concentrations, using data from cases with 0–10% mol_{H_2} toluene dopants, whereas trends for large toluene:H_2 blending ratios used

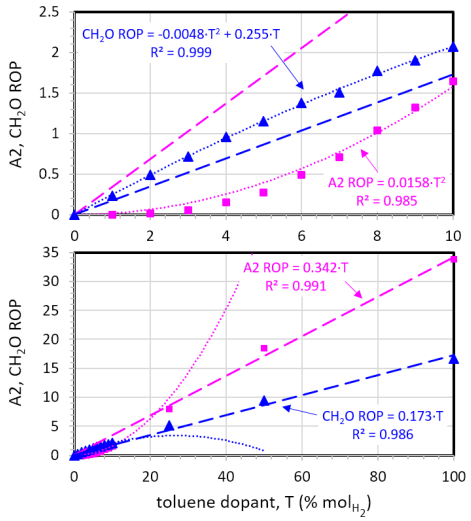

Fig. 7: Formaldehyde (CH_2O) and naphthalene (A2) production rate for small (top) and large (bottom) dopant concentrations. Dashed lines are trends using only toluene concentrations $\geq$10% mol_{H_2}.

data-points between 10–100% mol_{H_2} toluene concentrations (100% mol_{H_2} being 1:1 toluene:H_2). Comparison of trends for peak ROP of A2 and CH_2O for small and large toluene concentrations demonstrate that one regime cannot be used to predict the other. Peak ROP of both these species increase quadratically for dopant-level toluene addition, however these trends rapidly deviate from simulations for flames with toluene concentrations above 10% mol_{H_2}. This effect is more significant for the ROP of the larger A2 species, with the linear trend over-predicting the A2 ROP by a factor of $\sim$7 for a toluene concentration of 5% mol_{H_2}, whereas the linear prediction of CH_2O ROP overestimates by up to 30%. A similar distinction may be observed for the ratio of peak ROPs (supplied as Supplementary Data), with significantly different predictions produced using data from the dopant and blending regimes.

The decomposition of toluene (ROPs supplied as Supplementary Data) also differs between regimes. For large toluene concentrations, the endothermic reaction $A1CH_3 \leftrightarrow C_6H_5+CH_3$ favours C_6H_5 formation, however this is suppressed in the dopant regime. In the blending regime, C_6H_5, C_5H_5 and C_2H_2 are produced directly from $A1CH_2$. The C_6H_5 directly forms A1, other monocylcic aromatics and C_9H_7, an A2 precursor. Similarly, C_5H_5 forms C_2H_2 and C_3H_3, another A2 precursor. In contrast, production of C_6H_5, C_5H_5 and C_2H_2 are suppressed in the dopant regime, inhibiting both soot precursor formation and PAH growth via C_2H_2 addition.

The combination of conclusions drawn from Fig. 7 explain the near-absence of soot from the all-gaseous HT1-V case (in particular), with oxidation pathways dominating A2 and, hence, soot formation. In contrast, soot formation still occurs around droplets in the HT1-S dilute-spray-flame in regions where high local concentrations of toluene around droplets allow for the formation of A2 over CH_2O and – hence – soot production.

7. Conclusions

Measurements of turbulent H_2/N_2 flames doped with liquid or prevaporised toluene, complemented by laminar opposed-flow flame simulations has demonstrated substantial differences across a series of flames. Results demonstrate that soot volume fraction increases non-linearly with toluene dopant as a proportion of total H_2 fuel, with less than $\approx$3% mol_{H_2} resulting in little soot production in homogenous fuel mixtures. Toluene concentrations as low as 3–5% mol_{H_2}, however, result in significant soot loading with little impact on OH profiles. Distributions of soot and the location of peak soot volume fraction vary depending on the phase of the dopant, i.e. if the toluene is

introduced as a liquid in a dilute spray flame or as a prevaporised gas. In the former case, high local concentrations of toluene surrounding individual fuel droplets result in isolated regions of soot near the jet exit plane and delays the peak soot region, compared with the prevaporised dopant.

Finally, as representative intermediates in the oxidation of toluene or its further growth to PAHs, peak ROPs of CH_2O and A2 were analysed for different doping/blending fractions. Analyses highlight the chemical differences between the fuel blending and doping, which result in significant non-linearities in soot production, and consequently soot volume fraction and flame radiation. The competition between A2 formation and oxidation serves to explain the non-linear trends observed and measured experimentally. Results imply that doping hydrogen for increased radiative heat transfer should be considered separately to blending similar concentrations of hydrocarbon and hydrogen fuels.

Acknowledgements

The authors thank Dr Jingjing Ye for her original burner design. Support is acknowledged from the University of Adelaide with partial funding through the Australian Research Council (ARC) through the Discovery (DP) grant scheme and the Future Fuels CRC, through the Australian Governments Cooperative Research Centres Program: Project RP1.10-04.

References

[1] H. Guo, F. Liu, G. J. Smallwood, Ö. L. Gülder, Numerical study on the influence of hydrogen addition on soot formation in a laminar ethylene–air diffusion flame, Combust. Flame 145 (2006) 324–338.

[2] G. K. Lilik, H. Zhang, J. M. Herreros, D. C. Haworth, A. L. Boehman, Hydrogen assisted diesel combustion, Int. J. Hydrogen Energ. 35 (2010) 4382–4398.

[3] L. Arteaga Mendez, M. Tummers, E. van Veen, D. Roekaerts, Effect of hydrogen addition on the structure of natural-gas jet-in-hot-coflow flames, Proc. Combust. Inst. 35 (2015) 3557–3564.

[4] A. Pütün, A. Özcan, E. Pütün, Pyrolysis of hazelnut shells in a fixed-bed tubular reactor: yields and structural analysis of bio-oil, J. Anal. Appl. Pyrolysis 52 (1999) 33–49.

[5] S. Dooley, S. H. Won, M. Chaos, J. Heyne, Y. Ju, F. L. Dryer, K. Kumar, C.-J. Sung, H. Wang, M. A. Oehlschlaeger, R. J. Santoro, T. A. Litzinger, A jet fuel surrogate formulated by real fuel properties, Combust. Flame 157 (2010) 2333–2339.

[6] P. Pepiot-Desjardins, H. Pitsch, R. Malhotra, S. Kirby, A. Boehman, Structural group analysis for soot reduction tendency of oxygenated fuels, Combust. Flame 154 (2008) 191–205.

[7] W. O'Loughlin, A. Masri, A new burner for studying auto-ignition in turbulent dilute sprays, Combust. Flame 158 (2011) 1577–1590.

[8] P. O. Witze, S. Hochgreb, D. Kayes, H. A. Michelsen, C. R. Shaddix, Time-resolved laser-induced incandescence and laser elastic-scattering measurements in a propane diffusion flame, Appl. Opt. 40 (2001) 2443–2452.

[9] R. L. V. Wal, K. A. Jensen, Laser-induced incandescence: excitation intensity, Appl. Opt. 37 (1998) 1607–1616.

[10] B. Axelsson, R. Collin, P.-E. Bengtsson, Laser-induced incandescence for soot particle size measurements in premixed flat flames, Appl. Opt. 39 (2000) 3683–3690.

[11] F. Ossler, T. Metz, M. Aldén, Picosecond laser-induced fluorescence from gas-phase polycyclic aromatic hydrocarbons at elevated temperatures. I. Cell measurements, Appl. Phys. B 72 (2001) 465–478.

[12] J. Ye, P. R. Medwell, K. Kleinheinz, M. J. Evans, B. B. Dally, H. G. Pitsch, Structural Differences of Ethanol and DME Jet Flames in a Hot Diluted Coflow, Combust. Flame 192 (2018) 473–494.

[13] S. Kruse, J. Ye, Z. Sun, A. Attili, B. Dally, P. Medwell, H. Pitsch, Experimental investigation of soot evolution in a turbulent non-premixed prevaporized toluene flame, Proc. Combust. Inst. 37 (2019) 849–857.

[14] L. Cai, H. Pitsch, Optimized chemical mechanism for combustion of gasoline surrogate fuels, Combust. Flame 162 (2015) 1623–1637.

[15] F. Bisetti, G. Blanquart, M. E. Mueller, H. Pitsch, On the formation and early evolution of soot in turbulent nonpremixed flames, Combust. Flame 159 (2012) 317–335.

[16] M. J. Evans, P. R. Medwell, Z. Sun, A. Chinnici, J. Ye, Q. N. Chan, B. B. Dally, Downstream evolution of n-heptane/toluene flames in hot and vitiated coflows, Combust. Flame 202 (2019) 78–89.

[17] T. C. Lau, G. J. Nathan, Influence of Stokes number on the velocity and concentration distributions in particle-laden jets, J. Fluid Mech. 757 (2014) 432–457.